

## Mode structure of the $L3$ photonic crystal cavity

A. R. A. Chalcraft<sup>a)</sup> and S. Lam

*Department of Physics and Astronomy, The University of Sheffield, Sheffield S3 7RH, United Kingdom*

D. O'Brien and T. F. Krauss

*School of Physics and Astronomy, The University of St. Andrews, St. Andrews KY16 9SS, United Kingdom*

M. Sahin, D. Szymanski, D. Sanvitto, R. Oulton, M. S. Skolnick,  
A. M. Fox, and D. M. Whittaker

*Department of Physics and Astronomy, University of Sheffield, Sheffield S3 7RH, United Kingdom*

H.-Y. Liu and M. Hopkinson

*EPSRC National Centre for III-V Technologies, Department of Electronic and Electrical Engineering,  
University of Sheffield, Sheffield S1 3JD, United Kingdom*

(Received 7 March 2007; accepted 18 May 2007; published online 15 June 2007)

The authors investigate the multiple confined modes of GaAs  $L3$  photonic crystal air-bridge cavities, using single layers of InAs quantum dots as active internal light sources. Theoretical results for the energies, quality factors, and emission polarizations of the first five modes are compared to experimental data for cavities with lattice periods ranging from 240 to 270 nm. The authors also present in-plane field distributions for each mode. In addition to the well-known quality factor improvement of the fundamental mode, they show that outward displacement of the end-holes selectively redshifts modes with large end-hole-field overlaps, thus reordering the modes.

© 2007 American Institute of Physics. [DOI: [10.1063/1.2748310](https://doi.org/10.1063/1.2748310)]

The “ $L3$ ” defect was the first type of photonic crystal nanocavity in which quality factors in excess of  $10^4$  were obtained experimentally.<sup>1</sup> This nanocavity consists of a photonic crystal membrane with a line of three holes missing, as shown in Fig. 1(c). The high quality factors are obtained by displacing the end-holes of the cavity by a small amount, which reduces the radiation losses compared to cavities with undisplaced holes. Following the initial demonstration of high quality factors,  $L3$  defect cavities have been the subject of intense research for applications in cavity quantum electrodynamics (QED),<sup>2,3</sup> low-threshold lasing,<sup>4-7</sup> and control of ultrafast laser pulses.<sup>8</sup>

Reported work on the  $L3$  cavity has mainly concentrated on maximizing the quality factor  $Q$  of the fundamental mode, with the specific aim of optimizing the ratio of  $Q$  to the modal volume. A fact that is rarely discussed is that the  $L3$  cavity is capable of supporting a multitude of modes, the properties of which remain largely unexplored. The higher-order modes are important for the efficient pumping of nanocavity lasers,<sup>6</sup> and also for the selective excitation of quantum dots embedded within the cavity.<sup>9,10</sup>

In this letter we present an analysis of the mode structure of  $L3$  defects, in terms of mode energy, field profile, and emission polarization. We find a reordering of the modes when the end holes are displaced, predicted by our theoretical model and confirmed by experimental results. The improved understanding of the higher-order modes is useful for the design of more efficient lasers and for the observation of cavity QED effects from single quantum dots coupled to high  $Q$  nanocavities.

A scanning electron microscope image of a typical  $L3$  cavity is shown in Fig. 1(c). The cavities were fabricated in a GaAs membrane containing a single layer of InAs quantum

dots. Electron-beam lithography and chemically assisted ion beam etching were used to make hexagonal lattices of circular air holes, with lattice constants  $a$  ranging from 240–270 nm and nominal bulk fill factor  $f=0.29$ . A subset of the cavities had the holes at either end of the defect displaced outwards by  $s=0.15a$ , with the rest having no end-hole displacements (i.e.,  $s=0$ ). Air bridges of thickness  $d=140$  nm were fabricated by etching away a sacrificial  $\text{Al}_{0.85}\text{Ga}_{0.15}\text{As}$  layer of thickness 1500 nm using hydrofluoric acid.

We first present our theoretical studies of the cavity mode structure, which were performed by using a method similar to that used by Whittaker *et al.*,<sup>11</sup> and also by Andreani *et al.*<sup>12,13</sup> for slightly different systems. The calculations find the modes of patterned air-bridge structures using an expansion in a basis of the guided modes of an unpatterned membrane. The emission from the structure including its polarization is calculated by evaluating the coupling of each cavity mode to the scattering states of the unpatterned membrane.  $Q$  can then be found in terms of a first-order self-energy correction to the cavity mode energy. This method is very accurate for high  $Q$  modes, since they couple very weakly to scattering modes.

Previous work on waveguide mode field parities<sup>12,14</sup> concerned parities along the direction normal to the plane; the nature of the band gap for our chosen filling fraction dictates that all the confined states of our  $L3$  cavities are even in this direction (i.e., TE-like). Our structures are also symmetric along the  $x$  and  $y$  axes, allowing us to introduce identifying notation for the modes in terms of the in-plane parities of their  $E_x$  fields at the center of the membrane. We place the parity along the  $x$  axis above the parity along the  $y$  axis, and add a numerical index denoting their ordering in terms of energy. As the high  $Q$  fundamental mode has an  $E_x$  field of odd parity (along both in-plane axes) and it is the lowest energy mode with such a parity, we term it [ $\bar{1}$ ].  $E_y$

<sup>a)</sup>Electronic mail: a.chalcraft@shef.ac.uk

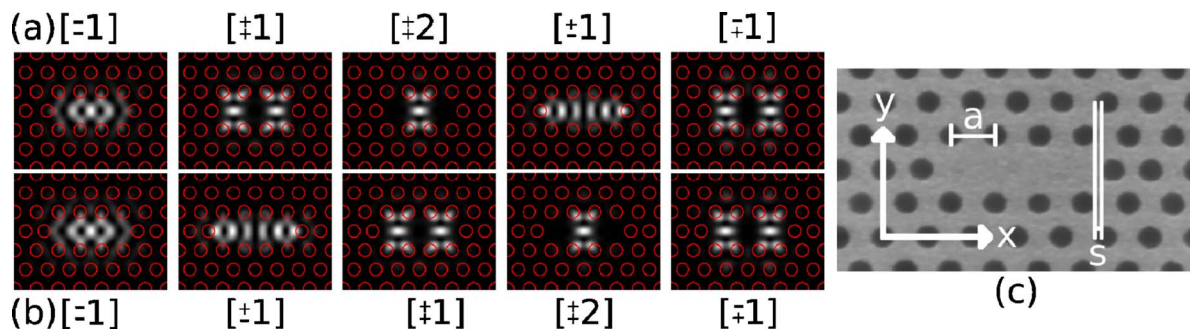


FIG. 1. (Color online) Calculated  $|E|^2$  intensity patterns for  $L3$  defects with  $a=240$  nm for (a)  $s=0$  and (b)  $s=0.15a$ . The notation used to label the modes refers to the in-plane parities of their  $E_x$  fields. Note that the mode ordering changes with the displacement of the end-holes. (c) Scanning electron microscope image of a typical  $L3$  cavity with lattice constant  $a=240$  nm, and end-holes outwardly displaced by  $s=0.15a$ . The arrows define the  $x$  and  $y$  directions as used throughout this letter.

parities can be determined by using the condition  $\nabla \cdot \mathbf{D}=0$ ; the  $E_y$  parity along each axis is the opposite of the corresponding  $E_x$  parity. From the in-plane parities, it is possible to infer information regarding near-normal emission. Doubly positive in-plane field parities are required for coupling to the exactly vertical scattering states of that field component. Negative parities force a cancellation in the overlap between the confined and scattering states, inhibiting vertical emission of the considered field component; thus,  $[\pm N]$  and  $[\mp N]$  states, respectively, favor  $x$ - and  $y$ -polarized vertical emission.  $[\pm N]$  and  $[\mp N]$  states provide no exactly vertical emission; to establish their dominant near-normal emission polarizations, it is necessary to consider coupling at nearby finite in-plane wave vectors, which are within the angular range of our experimental collection.

Calculated mode patterns for cavities with  $a=240$  nm are shown in Fig. 1. Figure 1(a) presents the results for a cavity with undisplaced holes (i.e.,  $s=0$ ), while Fig. 1(b) shows the equivalent results for a cavity with  $s=0.15a$ . For each mode, we plot the electric field intensity,  $|E|^2$  at the center of the membrane.

Consider first the modes shown in Fig. 1(a) for a cavity with  $s=0$ . The energies,  $Q$  factors, modal volumes, and dominant near-normal emission polarizations are given in Table I. Five modes were found in the range of 1.33–1.42 eV. Of these, the fundamental mode has the highest  $Q$ . Four higher energy modes are grouped together with energies of 0.07–0.09 eV higher than the fundamental (see Table I).

Now consider the modes of the structure with  $s=0.15a$  [Fig. 1(b)]. It is striking that the modes appear in a different order to those of the  $s=0$  structure [Fig. 1(a)]. The modes with strong  $E$  fields in the region of the displaced holes (i.e.,  $[\pm 1]$  and, to a lesser extent,  $[\mp 1]$ ) are strongly redshifted (see Table I), whereas those with minimal fields in that area (i.e., the  $[\pm 1]$ ,  $[\pm 2]$ ,  $[\mp 1]$  modes) are almost unaffected by end-hole displacement. We thus explain the reordering of the modes between  $s=0$  and  $s=0.15a$  in terms of end-hole-field overlap. It is also evident that the  $Q$  of the most heavily redshifted mode (i.e., the  $[\pm 1]$  mode) is significantly improved, as is widely known for the  $[\mp 1]$  mode.

In order to verify the predictions of our theoretical model, we have investigated the energy,  $Q$  factor, and polarization of the modes by performing photoluminescence (PL) experiments on the quantum dot layer embedded within the membranes. The structure was illuminated off-resonance with a HeNe laser at 633 nm, and the PL was collected in the direction normal to the sample surface using a microscope objective with a numerical aperture of 0.42. The PL spectra were then obtained with a spectrograph and charge coupled device detector. The sample was mounted in a helium flow cryostat at a temperature of  $\sim 10$  K.

Figure 2 shows the results of typical PL measurements on cavities with  $a=240$  nm for  $s=0$  and  $s=0.15a$ . The range of the PL measurements was restricted to 1.22–1.42 eV by the quantum dot emission spectra and the sensitivity of the detector. Within this range, we observed two modes for the

TABLE I. Calculated parameters of the modes for  $a=240$  nm illustrated in Fig. 1. Energy, mode energy;  $Q_{\text{th}}$ , theoretical quality factor;  $V$ , modal volume;  $n$ , energy dependent refractive index (Ref. 15);  $Q_{\text{ex}}$ , experimental quality factor of the modes identified in the PL spectra shown in Fig. 2; Polarization, dominant emission polarization expected near the normal to the plane. Modes are listed in order of increasing frequency.

$s/a$	Mode	Energy (eV)	$Q_{\text{th}}$	$Q_{\text{ex}}$	$V/(\lambda/n)^3$	Polarization
0	$[\mp 1]$	1.331 52	5 600	2 200	0.64	$y$
	$[\pm 1]$	1.405 38	440	520	0.67	$x$
	$[\pm 2]$	1.413 56	500	...	0.35	$x$
	$[\pm 1]$	1.414 08	710	...	0.72	$y$
	$[\mp 1]$	1.423 37	400	...	0.73	$x$
0.15	$[\mp 1]$	1.323 63	47 000	3 500	0.76	$y$
	$[\pm 1]$	1.380 53	2 100	1 300	0.78	$y$
	$[\mp 1]$	1.404 97	430	540	0.68	$x$
	$[\pm 2]$	1.412 76	510	...	0.36	$x$
	$[\mp 1]$	1.422 36	380	...	0.74	$x$

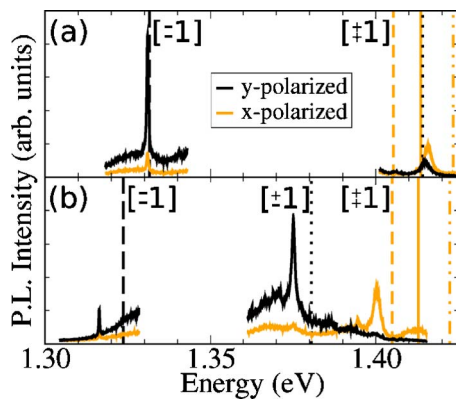


FIG. 2. (Color online) Typical experimental PL spectra for cavities with lattice constant  $a=240$  nm and end-hole displacements of (a)  $s=0$  and (b)  $s=0.15a$ . The lighter and darker spectra, respectively, show the experimental  $x$ -polarized and  $y$ -polarized cavity emission. The vertical lines denote theoretical mode energies taken from Table I, with line styles common to Fig. 3.

$s=0$  cavity and three for the cavity with  $s=0.15a$ . As predicted theoretically, the  $[-1]$  mode is redshifted and exhibits a higher  $Q$  for  $s=0.15a$  compared to  $s=0$  (see Table I). The highest measured  $Q$  values are well below the theoretical ones due to imperfections in the samples. In both samples the  $[-1]$  mode is linearly polarized along the  $y$  axis of the cavity, in agreement with results by other groups.<sup>3,7</sup>

In the cavity with  $s=0$ , the first higher-order mode ( $[+1]$ ) at 1.415 eV is polarized predominantly along the  $x$  axis [see Fig. 2(a)]. However, the  $[+1]$  mode is not the second mode of the  $s=0.15a$  cavity, but rather the third. The second is the  $y$ -polarized  $[-1]$  mode at 1.375 eV, which was the fourth mode of the  $s=0$  cavity, and has a reduced energy and enhanced  $Q$  for  $s=0.15a$ .

Figure 3 overlays experimental and theoretical mode energies for  $a=240$ –270 nm; strong agreement to within  $\pm 1\%$  is shown across the entire range, showing correct under-

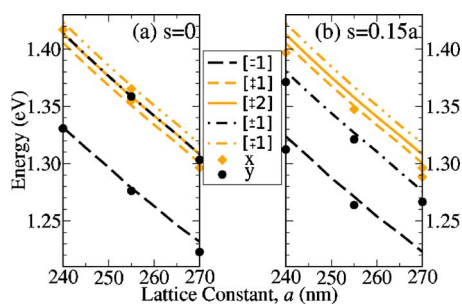


FIG. 3. (Color online) Energies of the modes for (a)  $s=0$  and (b)  $s=0.15a$ , as a function of lattice period. Lines and points, respectively, represent theoretical and mean experimental values.  $x$ -polarized and  $y$ -polarized modes appear lighter and darker, respectively.

standing of the modes. The energy shifts due to lattice constant did not significantly affect experimental  $Q$  factors, which suggests that the  $Q$  of the fundamental mode is not limited by absorption due to the quantum dots, wetting layer, or electronic surface states.

In conclusion, we have studied the mode structure of  $L3$  defects in photonic crystals both theoretically and experimentally. We show that end-hole displacement not only increases the  $Q$  factor of the fundamental mode but that it strongly redshifts those modes which have large end-hole-field overlaps, thus reordering the modes. We have calculated and experimentally verified emission polarizations, and presented in-plane field profiles for each mode. This understanding of the higher energy modes should be particularly useful for the selective excitation of emitters that are strongly coupled to the cavity, for example, in cavity QED experiments on single quantum dots in high  $Q$  nanocavities.

This research was supported by the EPSRC through program Grant No. GR/S76076/01 and the Quantum Information Processing Interdisciplinary Research Collaboration GR/S822176/01. One of the authors (M.S.) thanks TUBITAK for their financial support.

<sup>1</sup>Y. Akahane, T. Asano, B.-S. Song, and S. Noda, *Nature* (London) **425**, 944 (2003).

<sup>2</sup>T. Yoshie, A. Scherer, J. Hendrickson, G. Khitrova, H. M. Gibbs, G. Rupper, C. Ell, O. B. Shchekln, and D. G. Deppe, *Nature* (London) **432**, 200 (2004).

<sup>3</sup>W.-H. Chang, W.-Y. Chen, H.-S. Chang, T.-P. Hsieh, J.-I. Chyi, and T.-M. Hsu, *Phys. Rev. Lett.* **96**, 117401 (2006).

<sup>4</sup>J. Hendrickson, B. C. Richards, J. Sweet, S. Mosor, C. Christenson, D. Lam, G. Khitrova, H. M. Gibbs, T. Yoshie, A. Scherer, O. B. Shchekln, and D. G. Deppe, *Phys. Rev. B* **72**, 193303 (2005).

<sup>5</sup>M. Nomura, S. Iwamoto, K. Watanabe, N. Kumagai, Y. Nakata, S. Ishida, and Y. Arakawa, *Opt. Express* **14**, 6308 (2006).

<sup>6</sup>M. Nomura, S. Iwamoto, M. Nishioka, S. Ishida, and Y. Arakawa, *Appl. Phys. Lett.* **89**, 161111 (2006).

<sup>7</sup>S. Strauf, K. Hennessy, M. T. Rakher, Y.-S. Choi, A. Badolato, L. C. Andreani, E. L. Hu, P. M. Petroff, and D. Bouwmeester, *Phys. Rev. Lett.* **96**, 127404 (2006).

<sup>8</sup>T. Asano, W. Kunishi, B.-S. Song, and S. Noda, *Appl. Phys. Lett.* **88**, 151102 (2006).

<sup>9</sup>M. Nomura, S. Iwamoto, T. Nakaoka, S. Ishida, and Y. Arakawa, *Jpn. J. Appl. Phys., Part 1* **45**, 6091 (2006).

<sup>10</sup>M. Nomura, S. Iwamoto, T. Yang, S. Ishida, and Y. Arakawa, *Appl. Phys. Lett.* **89**, 241124 (2006).

<sup>11</sup>D. M. Whittaker, I. S. Culshaw, V. N. Astratov, and M. S. Skolnick, *Phys. Rev. B* **65**, 073102 (2002).

<sup>12</sup>L. C. Andreani and Mario Agio, *IEEE J. Quantum Electron.* **38**, 891 (2002).

<sup>13</sup>L. C. Andreani and D. Gerace, *Phys. Rev. B* **73**, 235114 (2006).

<sup>14</sup>S. G. Johnson, S. Fan, P. R. Villeneuve, and J. D. Joannopoulos, *Phys. Rev. B* **60**, 5751 (1999).

<sup>15</sup>Calculated in the limit of pure GaAs using the approximate formula due to J. T. Boyd, *IEEE J. Quantum Electron.* **8**, 788 (1972).